Charge Noise Spectroscopy Using Coherent Exchange Oscillations in a Singlet-Triplet Qubit

Electrometry using coherent exchange oscillations in a singlet-triplet qubit

O. E. Dial,[1] M. D. Shulman,[1] S. P. Harvey,[1] H. Bluhm,[1,2] V. Umansky,[3] and A. Yacoby[1]

[1] *Department of Physics, Harvard University, Cambridge, MA, 02138, USA*
[2] *Current Address: 2nd Institute of Physics C, RWTH Aachen University, 52074 Aachen, Germany*
[3] *Braun Center for Submicron Research, Department of Condensed Matter Physics, Weizmann Institute of Science, Rehovot 76100 Israel*

(Dated: April 9, 2013)

Two level systems that can be reliably controlled and measured hold promise as qubits both for metrology and for quantum information science (QIS). Since a fluctuating environment limits the performance of qubits in both capacities, understanding the environmental coupling and dynamics is key to improving qubit performance. We show measurements of the level splitting and dephasing due to voltage noise of a GaAs singlet-triplet qubit during exchange oscillations. Unexpectedly, the voltage fluctuations are non-Markovian even at high frequencies and exhibit a strong temperature dependence. The magnitude of the fluctuations allows the qubit to be used as a charge sensor with a sensitivity of $2 \times 10^{-8} e/\sqrt{\text{Hz}}$, two orders of magnitude better than a quantum-limited RF single electron transistor (RF-SET). Based on these measurements we provide recommendations for improving qubit coherence, allowing for higher fidelity operations and improved charge sensitivity.

PACS numbers: 85.35.Be 03.67.-a 07.50.Ls 76.60.Lz 07.50.Hp

Two level quantum systems (qubits) are emerging as promising candidates both for quantum information processing [1] and for sensitive metrology [2, 3]. When prepared in a superposition of two states and allowed to evolve, the state of the system precesses with a frequency proportional to the splitting between the states. However, on a timescale of the coherence time, T_2, the qubit loses its quantum information due to interactions with its noisy environment. This causes qubit oscillations to decay and limits the fidelity of quantum control and the precision of qubit-based measurements. In this work we study singlet-triplet (S-T_0) qubits, a particular realization of spin qubits [4–11], which store quantum information in the joint spin state of two electrons[12–14]. We form the qubit in two gate-defined lateral quantum dots (QD) in a GaAs/AlGaAs heterostructure (Fig. 1**a**). The QDs are depleted until there is exactly one electron left in each, so that the system occupies the so-called $(1,1)$ charge configuration. Here (n_L, n_R) describes a double QD with n_L electrons in the left dot and n_R electrons in the right dot. This two-electron system has four possible spin states: $|S\rangle$, $|T_+\rangle$, $|T_0\rangle$, and $|T_-\rangle$. The $|S\rangle$,$|T_0\rangle$ subspace is used as the logical subspace for this qubit because it is insensitive to homogeneous magnetic field fluctuations and is manipulable using only pulsed DC electric fields [12, 13, 15]. The relevant low-lying energy levels of this qubit are shown in Fig. 1**c**. Two distinct rotations are possible in these devices: rotations around the x-axis of the Bloch sphere driven by difference in magnetic field between the QDs, ΔB_z(provided in this experiment by feedback-stabilized hyperfine interactions[16]), and rotations around the z-axis driven by the exchange interaction, J (Fig. 1**b**) [17]. A $|S\rangle$ can be prepared quickly with high fidelity by exchanging an electron with the QD leads, and the projection of the state of the qubit along the z-axis can be measured using RF reflectometery with an adjacent sensing QD (green arrow in Fig. 1**a**)[18, 19].

Previous work on S-T_0 qubits focused almost entirely on x (ΔB_Z) rotations, which are dephased by fluctuations in the nuclear bath [20–22]. In this work, we focus on the exchange interaction, which creates a splitting, J, between the $|S\rangle$ and $|T_0\rangle$ states once the $(1,1)$ and $(0,2)|S\rangle$ states of the double QD are brought near resonance (Fig. 1**c**). The value of J depends on the energy detuning, ϵ, between the QDs. The exchange interaction drives single qubit rotations in S-T_0 [13] and exchange-only [23, 24] qubits and is the foundation for two-qubit operations in single spin, S-T_0, and exchange-only qubits ([5, 25–28]). Exchange oscillations are dephased by fluctuations in J (Fig. 1**c**) driven, for example, by ϵ (voltage) fluctuations between the dots with a tunable sensitivity proportional to $dJ/d\epsilon$ (Fig. 1**d**) [29]. We will show that this controllable sensitivity is a useful experimental tool for probing the noise bath dynamics. Previous studies have shown the decay of exchange oscillations within a few π rotations [13, 30], but a detailed study of the nature of the noise bath giving rise to this decay is still lacking. In this work, using nuclear feedback to control x-rotations, we systematically explore the low frequency noise portion of the voltage noise bath and its temperature dependence, as well as introduce a new Hahn-echo based measurement of the high frequency components of the voltage noise and its temperature dependence.

The simplest probe of J and its fluctuations is a free induction decay (FID) experiment, in which the qubit is allowed to freely precess for a time t under the influence of the exchange splitting. For FID measurements, we use a $\pi/2$ pulse around the x-axis to prepare and readout the state of the qubit along the y-axis (Fig. 2**a**, Fig. **S1**). Fig. 2**b** shows qubit oscillations as a function of

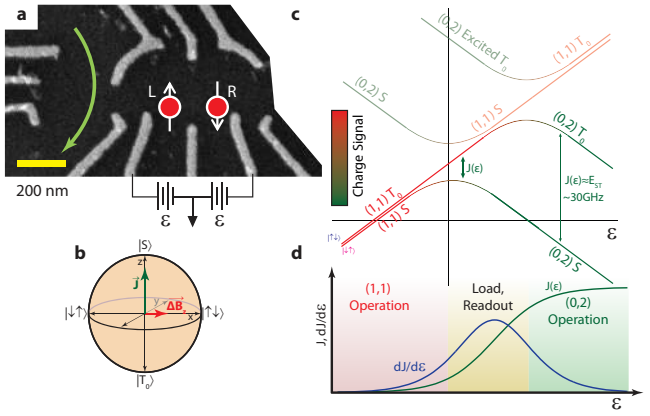

FIG. 1. The device used in these measurements is a gate-defined S-T_0 qubit with an integrated RF sensing dot. **a** The detuning ϵ is the voltage applied to the dedicated high-frequency control leads pictured. **b**, The Bloch sphere that describes the logical subspace of this device features two rotation axes (J and ΔB_Z) both controlled with DC voltage pulses. **c**, An energy diagram of the relevant low-lying states as a function of ϵ. States outside of the logical subspace of the qubit are grayed out. **d**, $J(\epsilon)$ and $dJ/d\epsilon$ in three regions; the $(1,1)$ region where J and $dJ/d\epsilon$ are both small and S-T_0 qubits are typically operated, the transitional region where J and $dJ/d\epsilon$ are both large where the qubit is loaded and measured, and the $(0,2)$ region where J is large but $dJ/d\epsilon$ is small and large quality oscillations are possible.

t for many different values of ϵ. By measuring the period of these oscillations with t we extract $J(\epsilon)$, and we calculate $dJ/d\epsilon$ by fitting $J(\epsilon)$ to a smooth function and differentiating (Fig. 2**c**). For negative ϵ (small J), we empirically find across many devices and tunings that J is well described by $J(\epsilon) \simeq J_0 + J_1 exp(-\epsilon/\epsilon_0)$.

The oscillations in these FID experiments decay due to voltage noise from DC up to a frequency of approximately $1/t$. As the relaxation time, T_1 is in excess of 100μs in this regime, T_1 decay is not an important source of decoherence (Fig. **S4**). The shape of the decay envelope and the scaling of coherence time with $dJ/d\epsilon$ (which effectively changes the magnitude of the noise) reveal information about the underlying noise spectrum. White (Markovian) noise, for example, results in an exponential decay of e^{-t/T_2^*} where $T_2^* \propto (dJ/d\epsilon)^{-2}$ is the inhomogeneously broadened coherence time [31]. However, we find that the decay is Gaussian (Fig. 2**d**) and that T_2^* (black line in Fig. 2**e**) is proportional to $(dJ/d\epsilon)^{-1}$ (red solid line in Fig. 2**e**) across two orders of magnitude of T_2^*. Both of these findings can be explained by quasistatic noise, which is low frequency compared to $1/T_2^*$. In such a case, one expects an amplitude decay of the form $\exp\left[-(t/T_2^*)^2\right]$, where $T_2^* = \frac{1}{\sqrt{2}\pi(dJ/d\epsilon)\epsilon_{RMS}}$ and ϵ_{RMS} is the root-mean-squared fluctuation in ϵ (Eq. **S3**). From the ratio of T_2^* to $(dJ/d\epsilon)^{-1}$, we calculate $\epsilon_{RMS} = 8\mu$V in our device. At very negative ϵ, J becomes smaller than ΔB_z, and nuclear noise limits T_2^* to approximately 90ns, which is consistent with previous work [16]. We confirm that this effect explains deviations of T_2^* from $(dJ/d\epsilon)^{-1}$ by using a model that includes the independently measured $T_{2,nuclear}^*$ and ΔB_z (Eq. **S1**) and observe that it agrees well with measured T_2^* at large negative ϵ (dashed red line in Fig. 2**e**).

Since we observe J to be approximately an exponential function of ϵ, $(dJ/d\epsilon \sim J)$, we expect and observe the quality (number of coherent oscillations) of these FID oscillations, $Q \equiv JT_2^*/2\pi \sim J(dJ/d\epsilon)^{-1}$, to be approximately constant regardless of ϵ. However, when ϵ is made very positive and J is large, an avoided crossing occurs between the $(1,1)|T_0\rangle$ and the $(0,2)|T_0\rangle$ state, making the $(0,2)|S\rangle$ and $(0,2)|T_0\rangle$ states electrostatically virtually identical. Here, as ϵ is increased, J increases but $dJ/d\epsilon$ decreases(Fig. 1**d**), allowing us to probe high quality exchange rotations and test our charge noise model in a regime that has never before been explored.

Using a modified pulse sequence that changes the clock frequency of our waveform generators to achieve picosecond timing resolution (Fig. **S1**)), we measure exchange oscillations in $(0,2)$ as a function of ϵ and time (Fig. 2**e**) and we extract both J (Fig. 2**c**) and T_2^* (Fig. 2**d**) as a function of ϵ. Indeed, the predicted behavior is observed: for moderate ϵ we see fast oscillations that decay after a few ns, and for the largest ϵ we see even faster oscillations that decay slowly. Here, too, we observe that $T_2^* \propto (\frac{dJ}{d\epsilon})^{-1}$ (Fig. 2**d**), which indicates that FID oscillations in $(0,2)$ are also primarily dephased by low frequency voltage noise. We note, however, that we extract a different constant of proportionality between T_2^* and $(dJ/d\epsilon)^{-1}$ for $(1,1)$ and $(0,2)$. This is expected given that the charge distributions associated with the qubit states are very different in these two regimes and thus have different sensitivities to applied electric fields. We note that in the regions of largest $dJ/d\epsilon$ (near $\epsilon = 0$), T_2^* is shorter than the rise time of our signal generator and we systematically underestimate J and overestimate T_2^* (Fig. **S1**).

The above measurements indicate that the dephasing during FID experiments in both $(1,1)$ and $(0,2)$ arises overwhelmingly due to low frequency (non-Markovian) noise, and the observed linear dependence of T_2^* on $(dJ/d\epsilon)^{-1}$ strongly suggests that ϵ noise is indeed responsible for the observed dephasing, as these data rule out dephasing from other mechanisms in most realistic situations (see supplement sec. 5). In the presence of such low frequency noise, the addition of a π-pulse halfway through the free evolution can partially decouple the qubit from its noisy environment. Such a "Hahn-echo" [32] sequence prolongs coherence, which is useful for complex quantum operations [25], sensitive detection [33], and probing higher-frequency portions of the voltage noise bath. Rather than being sensitive to noise from DC to $1/\tau$ where τ is the total evolution time, these echo

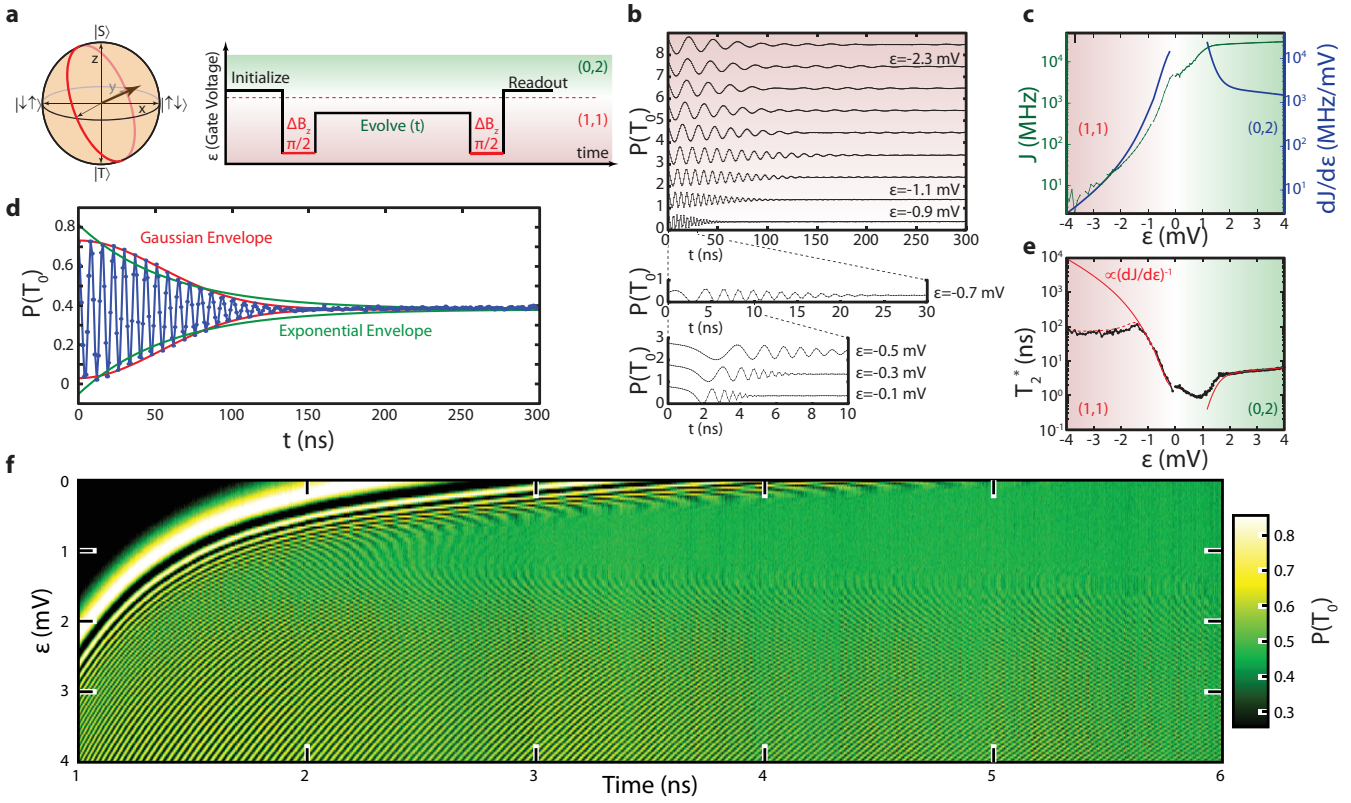

FIG. 2. Ramsey oscilllations reveal low frequency enivronmental dynamics. **a**, The pulse sequence used to measure exchange oscillations uses a stabilized nuclear gradient to prepare and readout the qubit and gives good contrast over a wide range of J. **b**, Exchange oscillations measured over a variety of detunings ϵ and timescales consistently show larger T_2^* as $dJ/d\epsilon$ shrinks until dephasing due to nuclear fluctuations sets in at very negative ϵ. **c**, Extracted values of J and $dJ/d\epsilon$ as a function of ϵ. **d**, The decay curve of FID exchange oscillations shows Gaussian decay. **e**, Extracted values of T_2^* and $dJ/d\epsilon$ as a function of ϵ. T_2^* is proportional to $(dJ/d\epsilon)^{-1}$, indicating that voltage noise is the cause of dephasing of charge oscillations. **f**, Charge oscillations measured in $(0,2)$. This figure portrays the three basic regions we can operate our device in: a region of low frequency oscillations and small $dJ/d\epsilon$, a region of large frequency oscillations and large $dJ/d\epsilon$, and a region where oscillations are fast but $dJ/d\epsilon$ is comparatively small.

sequences have a noise sensitivity peaked at $f \approx 1/\tau$ and a reduced sensitivity at lower frequencies.

In our echo measurements, we select a fixed ϵ inside $(1,1)$ for the free evolutions, and we sweep the length of the evolution following the π-pulse time by small increments δt to reveal an echo envelope (Fig. 3**a-b**). The maximum amplitude of this observed envelope reveals the extent to which the state has dephased during the echo process, while the Gaussian shape and width of the envelope arise from an effective single-qubit rotation for a time δt, and thus reflect the same T_2^* and low frequency noise measured in FID experiments. We note that this exchange echo is distinct from the echo measurements previously performed in singlet-triplet qubits[20–22] in that we use ΔB_z rotations to echo away voltage noise, rather than J rotations to echo away noise in the nuclear bath.

The use of Hahn echo dramatically improves coherence times, with T_2^{echo} (the τ at which the observed echo amplitude has decayed by $1/e$) as large as 9 μs, corresponding to qualities ($Q \equiv T_2^{echo} J/2\pi$) larger than 600 (Fig. 3**c**). If at high frequencies (50kHz-1MHz) the voltage noise were white (Markovian), we would observe exponential decay of the echo amplitude with τ. However, we find that the decay of the echo signal is non-exponential (Fig. 3**d**), indicating that even in this relatively high-frequency band being probed by this measurement, the noise bath is not white.

A simple noise model that can account for this decay includes a mixture of white and $1/f$ noise, $S_\epsilon(f) = A + B/f$, which leads to an echo amplitude decay $exp(-\tau/C_0 - \tau^2/C_1)$ [31], where $C_{0,1}$ are functions of the noise power. Since $C_{0,1}$ are both proportional to $(dJ/d\epsilon)^{-2}$, we expect the ratio $C_0/C_1 \propto A/B$ to be independent of $dJ/d\epsilon$. While this decay accurately describes the decay for a single value of ϵ, as we change ϵ (and therefore $dJ/d\epsilon$), we find that the ratio A/B changes, indicating that this model is inconsistent with our data

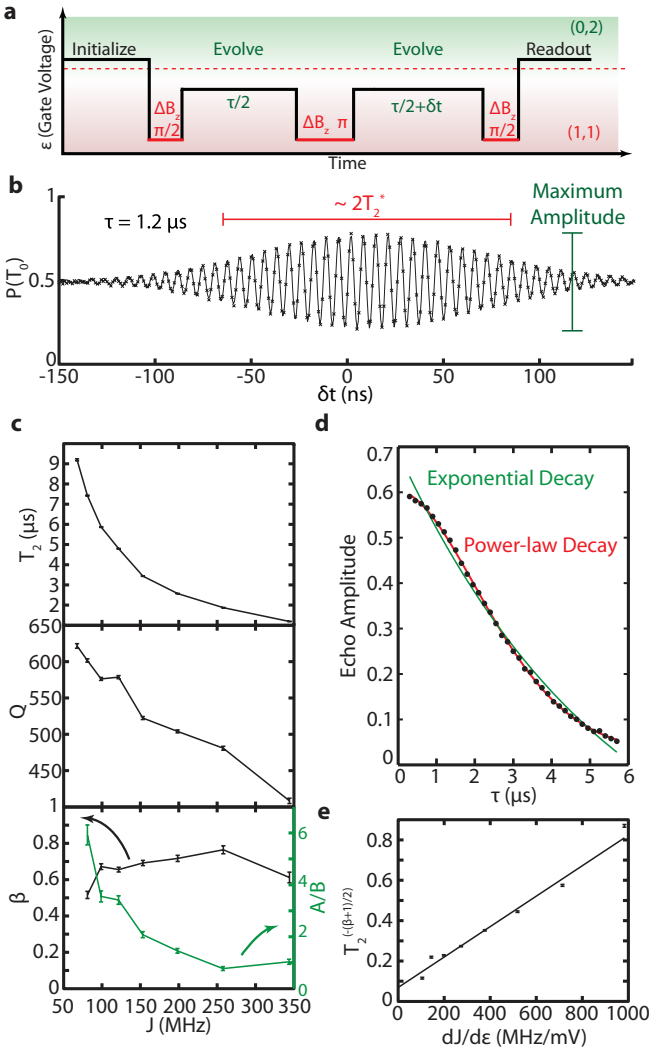

FIG. 3. Spin-echo measurements reveal high frequency bath dynamics. **a**, The pulse sequence used to measure exchange echo rotations. **b**, A typical echo signal. The overall shape of the envelope reflects T_2^*, while the amplitude of the envelope as a function of τ (not pictured) reflects T_2^{echo}. **c**, T_2^{echo} and $Q \equiv JT_2^{echo}/2\pi$ as a function of J. A comparison of the two noise models: power law and a mixture of white and $1/f$ noise. Noise with a power law spectrum fits over a wide range of frequencies (constant β), but the relative contributions of white and $1/f$ noise change as a function of ϵ. **d**, A typical echo decay is non-exponential but is well fit by $\exp(-(\tau/T_2^{echo})^{\beta+1})$. **e**, T_2^{echo} varies with $dJ/d\epsilon$ in a fashion consistent with dephasing due to power law voltage fluctuations.

because the relative contributions of white and $1/f$ noise change (Fig. 3**c**). Alternatively, we consider a power law noise model $S_\epsilon(f) = \frac{S_0}{f^\beta}$, which leads to an echo amplitude decay $exp(-(\tau/T_2^{echo})^{\beta+1})$. With this model we expect β to be independent of $dJ/d\epsilon$, and we indeed observe $\beta \approx 0.7$ for all values of ϵ (Fig. 3**c**), indicating that this model can adequately describe our observed

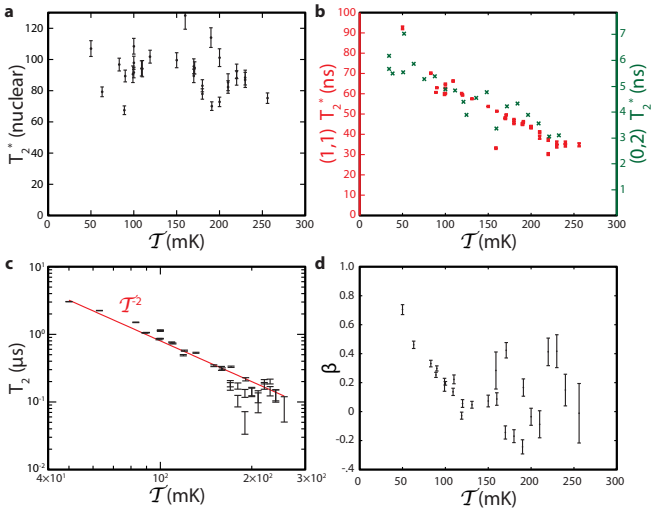

FIG. 4. Temperature dependence indicates the noise leading to dephasing originates near or inside the device. **a**, $T^*_{2,nuclear}$ does not depend significantly on $\mathcal{T}$. **b**, T_2^* in $(1,1)$ (red squares) and $(0,2)$ (green crosses) has the same, weak, scaled dependence on $\mathcal{T}$. **c**, T_2^{echo} shows a strong temperature dependence near $\mathcal{T}^2$ (red line) across over an order of magnitude in coherence times. **e**, As $\mathcal{T}$is increased, β approaches zero indicating the noise leading to decoherence becomes nearly white. Uncertainties in β are larger at higher temperatures due to the fast decay of the echo.

noise from approximately 50 kHz to 1 MHz. We further confirm that the observed dephasing is consistent with voltage noise by checking T_2^{echo} has the expected dependence on $dJ/d\epsilon$, namely, $T_2^{echo} \propto (dJ/d\epsilon)^{\frac{-2}{\beta+1}}$ (Fig. 3**e**). From the scale factor, we deduce that the noise is well approximated by $S_\epsilon(f) = 8\times10^{-16}\frac{\mathrm{V}^2}{\mathrm{Hz}}\left(\frac{1\mathrm{Hz}}{f}\right)^{0.7}$ from approximately 50 kHz to 1 MHz, corresponding to ϵ noise of 0.2 nV/$\sqrt{\mathrm{Hz}}$ at 1 MHz. We note that this noise exceeds that accounted for by known sources of noise present in the experiment, including instrumental noise on the device gates and Johnson noise of the wiring. The RMS noise deduced from our FID measurements exceeds that expected from this power-law noise; there is excess noise at very low frequencies in the device.

Thus far, we have explored the voltage noise bath at the base temperature of our dilution refrigerator ($\mathcal{T}\approx$50 mK). We gain additional insight into the properties of the voltage noise by studying its temperature dependence. For the nuclear bath, attainable temperatures in dilution refrigerators are much larger than the nuclear Zeeman splitting and no temperature dependence is expected. This is confirmed by measuring $T^*_{2,nuclear}$, the dephasing time for FID rotations in the stabilized nuclear gradient field (at J=0) as a function of $\mathcal{T}$(Fig. 4**a**).

By contrast, T_2^* in $(1,1)$ and $(0,2)$ show unexpected temperature dependences (Fig. 4**b**). These have the same scaled temperature dependence: $T^*_{2,(1,1)}(\mathcal{T}) \propto$

$T^*_{2,(0,2)}(\mathcal{T})$, suggesting the loss of coherence is due to the same mechanism, presumably increased voltage noise, in both instances. In both cases T_2^* is roughly linear with $\mathcal{T}$, indicating that only small gains are likely to be made in the quality of FID-based rotations by reducing $\mathcal{T}$. By comparison, T_2^{echo} shows a strong dependence of $T_2^{echo} \propto \mathcal{T}^{-2}$ (Fig. 4**c**). As $\mathcal{T}$is increased, the observed noise becomes increasingly white (frequency independent) (Fig. 4**d**), though measurements of β become inaccurate at large $\mathcal{T}$where T_2^{echo} is small. We note that the underlying mechanism of this temperature dependence is currently unknown, however the dependence of the observed dephasing on temperature strongly suggests that the noise originates within the device rather than the experimental apparatus. Lower temperatures carry a double benefit for echo coherence; the noise becomes both smaller and more non-Markovian, thereby increasing coherence times and extending the potential for multi-pulse dynamical decoupling sequences to mitigate the effects of the noise [34, 35]. This trend shows no indication of saturating at low temperatures; it appears likely much longer coherence times are attainable by reducing temperatures with more effective refrigeration (Fig. **S3**).

Operating at base temperature and using the Hahn echo sequence described above, we observe a voltage sensitivity of 0.2 nV/$\sqrt{\text{Hz}}$ at 1 MHz, which suggests that the qubit can be used as a sensitive electrometer at this frequency. In order to compare to other electrometers, we convert our voltage sensitivity into a charge sensitivity of 2×10^{-8}e/$\sqrt{\text{Hz}}$ by dividing by the Coulomb blockade peak spacing, 10mV. This value is nearly two orders of magnitude better than the theoretical limits for RF-SETs[36], and is limited only by T_2^{echo}, which the data suggest can be improved.

Using both FID and echo measurements, we have characterized the exchange interaction and presented experimental evidence that exchange rotations in S-T_0 qubits dephase due to voltage noise. These measurements reveal that the voltage noise bath that couples to the qubit is non-Markovian and establish baseline noise levels for S-T_0 qubits. We suggest that further improvements in operation fidelity and charge sensitivity are possible by reducing $\mathcal{T}$, using more complex pulse sequences such as CPMG [34] and UDD [35], and performing operations at larger J and $dJ/d\epsilon$ to move to a higher frequency portion of the noise spectrum with potentially lower noise. In particular, because two-qubit operations in S-T_0 qubits rely heavily on exchange echo [25], our data show a path forward for increasing gate fidelities in these devices and generating higher quality entangled states. Lastly, the metrological capabilities of the S-T_0 qubit may be further improved by harnessing the power of entanglement and measuring simultaneously with many qubits[37].

This work is supported through the ARO, "Precision Quantum Control and Error-Suppressing Quantum Firmware for Robust Quantum Computing" and the IARPA "Multi-Qubit Coherent Operations (MQCO) Program". This work was partially supported by the US Army Research Office under Contract Number W911NF-11-1-0068. This work is sponsored by the United States Department of Defence. The views and conclusions contained in the document are those of the authors and should not be interpreted as representing the official policies, either expressly or implied, of the U. S. Government. This work was performed in part at the Center for Nanoscale Systems (CNS), a member of the National Nanotechnology Infrastructure Network (NNIN), which is supported by the National Science Foundation under NSF award no. ECS-0335765. CNS is part of Harvard University.

[1] D. DiVincenzo, Fortschr. Phys. **48**, 771 (2000).
[2] B. M. Chernobrod and G. P. Brerman, Journal of Applied Physics **97**, 014903 (2005).
[3] P. Maletinsky, S. Hong, M. S. Grinolds, B. Hausmann, M. D. Lukin, R. L. Walsworth, M. Loncar, and A. Yacoby, Nature Nanotechnology **7**, 320 (2012).
[4] R. Hanson, L. P. Kouwenhoven, J. R. Petta, S. Tarucha, and L. M. K. Vandersypen, Rev. Mod. Phys. **79**, 1217 (2007).
[5] D. Loss and D. P. DiVincenzo, Phys. Rev. A **57**, 120 (1998).
[6] F. H. L. Koppens, C. Buizert, K. J. Tielrooij, I. T. Vink, K. C. Nowack, T. Meunier, L. P. Kouwenhoven, and L. M. K. Vandersypen, Nature **442**, 766 (2006).
[7] M. Pioro-Ladriere, T. Obata, Y. Tokura, Y. S. Shin, T. Kubo, K. Yoshida, T. Taniyama, and S. Tarucha, Nature Physics **4**, 776 (2008).
[8] K. C. Nowack, F. H. L. Koppens, Y. V. Nazarov, and L. M. K. Vandersypen, Science **318**, 1430 (2007).
[9] M. Pioro-Ladriere, Y. Tokura, T. Kubo, and S. Tarucha, Appl. Phys. Lett. **90**, 024105 (2007).
[10] H. O. H. Churchill, F. Kuemmeth, J. W. Harlow, A. J. Bestwick, E. I. Rashba, K. Flensberg, C. H. Stwertka, T. Taychatanapat, S. K. Watson, and C. M. Marcus, Phys. Rev. Lett. **102**, 166802 (2009).
[11] S. Nadj-Perfe, S. M. Frolov, E. P. A. M. Bkkers, and L. P. Kouwenhoven, Nature **468**, 1084 (2010).
[12] J. Levy, Phys. Rev. Lett. **89**, 147902 (2002).
[13] J. R. Petta, A. C. Johnson, J. M. Taylor, E. A. Laird, A. Yacoby, M. D. Lukin, C. M. Marcus, M. P. Hanson, and A. C. Gossard, Science **309**, 2180 (2005).
[14] J. M. Taylor, J. R. Petta, A. C. Johnson, A. Yacoby, C. M. Marcus, and M. D. Lukin, Phys. Rev. B **76**, 035315 (2007).
[15] J. M. Taylor, H.-A. Engel, W. Dür, A. Yacoby, C. M. Marcus, P. Zoller, and M. D. Lukin, Nature Physics **1**, 177 (2005).
[16] H. Bluhm, S. Foletti, D. Mahalu, V. Umansky, and A. Yacoby, Phys. Rev. Lett. **105**, 216803 (2010).
[17] S. Foletti, H. Bluhm, D. Mahalu, V. Umansky, and A. Yacoby, Nature Physics **5**, 903 (2009).
[18] D. J. Reilly, C. M. Marcus, M. P. Hanson, and A. C.

Gossard, Appl. Phys. Lett. **91**, 162101 (2007).
[19] C. Barthel, D. J. Reilly, C. M. Marcus, M. P. Hanson, and A. C. Gossard, Phys. Rev. Lett. **103**, 160503 (2009).
[20] H. Bluhm, S. Foletti, I. Neder, M. S. Rudner, D. Mahalu, V. Umansky, and A. Yacoby, Nature Physics **7**, 109 (2011).
[21] C. Barthel, J. Medford, C. M. Marcus, M. P. Hanson, and A. C. Gossard, Phys. Rev. Lett. **105**, 266808 (2010).
[22] J. Medford, L. Cywiński, C. Barthel, C. M. Marcus, M. P. Hanson, and A. C. Gossard, Phys. Rev. Lett. **108**, 086802 (2012).
[23] E. A. Laird, J. M. Taylor, D. P. DiVincenzo, C. M. Marcus, M. P. Hanson, and A. C. Gossard, Phys. Rev. B **82**, 075403 (2010).
[24] L. Gaudreau, G. Granger, A. Kam, G. C. Aers, S. A. S. andP. Zawadzki, M. Pioro-Ladrire, Z. R. Wasilewski, and A. S. Sachrajda, Nature Physics **8**, 54 (2011).
[25] M. D. Shulman, O. E. Dial, S. P. Harvey, H. Bluhm, V. Umansky, and A. Yacoby, Science **336**, 202 (2012).
[26] I. van Weperen, B. D. Armstrong, E. A. Laird, J. Medford, C. M. Marcus, M. P. Hanson, and A. C. Gossard, Phys. Rev. Lett. **107**, 030506 (2011).
[27] R. Brunner, Y.-S. Shin, T. Obata, M. Pioro-Ladrière, T. Kubo, K. Yoshida, T. Taniyama, Y. Tokura, and S. Tarucha, Phys. Rev. Lett. **107**, 146801 (2011).
[28] K. C. Nowack, M. Shafiei, M. Laforest, G. E. D. K. Prawiroatmodjo, L. R. Schreiber, C. Reichl, W. Wegscheider, and L. M. K. Vandersypen, Science **333**, 1269 (2011).
[29] D. Culcer, X. Hu, and S. D. Sarma, Appl. Phys. Lett **95**, 073102 (2009).
[30] B. M. Maune, M. G. Borselli, B. Huang, T. D. Ladd, P. W. Deelman, K. S. Holabird, A. A. Kiselev, I. Alvarado-Rodriguez, R. S. Ross, A. E. Schmitz, M. Sokolich, C. A. Watson, M. F. Gyure, and A. T. Hunter, Nature **481**, 344 (2011).
[31] L. Cywinski, R. M. Lutchyn, C. P. Nave, and S. D. Sarma, Phys. Rev. B **77**, 174509 (2008).
[32] E. L. Hahn, Phys. Rev. **80**, 580 (1950).
[33] J. R. Maze, P. L. Stanwix, J. S. Hodges, S. Hong, J. M. Taylor, P. Cappellaro, L. Jian, M. V. G. Dutt, E. Togan, A. S. Zibrov, A. Yacoby, R. L. Walsworth, and M. D. Lukin, Nature **455**, 644 (2008).
[34] H. Y. Carr and E. M. Purcell, Phys. Rev. **94**, 630 (1954).
[35] G. S. Uhrig, Phys. Rev. Lett. **98**, 100504 (2007).
[36] M. H. Devoret and R. J. Schoelkopf, Nature **406**, 1039 (2000).
[37] V. Giovannetti, S. Lloyd, and L. Maccone, Nature Photonics **5**, 222 (2011).

Supplemental Material for "Electrometry Using Coherent Exchange Oscillations in a Singlet-Triplet Qubit"

O. E. Dial,[1] M. D. Shulman,[1] S. P. Harvey,[1] H. Bluhm,[1,2] V. Umansky,[3] and A. Yacoby[1]

[1] *Department of Physics, Harvard University, Cambridge, MA, 02138, USA*
[2] *Current Address: 2nd Institute of Physics C, RWTH Aachen University, 52074 Aachen, Germany*
[3] *Braun Center for Submicron Research, Department of Condensed Matter Physics, Weizmann Institute of Science, Rehovot 76100 Israel*

(Dated: April 9, 2013)

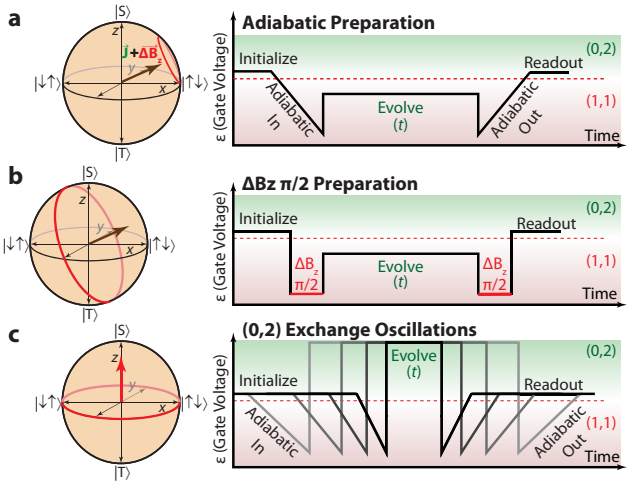

FIG. 1. **a**, The pulse sequence traditionally used to measure exchange oscillations in $(1,1)$ employs adiabatic preparation and readout but suffers reduced visibility when J becomes comparable to ΔB_Z. Red circles show the path of the state vector on the Bloch sphere during the exchange rotation for each sequence. **b**, We use a feedback-controlled nuclear gradient to prepare and readout on the y-axis, which provides good visibility for all values of J. **c**, The pulse sequence used to measure exchange oscillations in $(0,2)$ uses adiabatic preparation and readout and "stretches" the pulse by changing the waveform generator clock rate.

MEASURING $J(\epsilon)$

Previously[13,30], exchange oscillations were measured inside of (1,1) by preparing a $|S\rangle$, adiabatically turning J off to prepare a state on the x-axis of the Bloch sphere and then turning J on again to allow the qubit state to rotate around the z-axis. Finally, to map the x-axis of the Bloch sphere back to the z-axis for readout J is turned off suddenly and then adiabatically turned back on again (Fig. S1**a**). This allows measurements without a stabilized nuclear gradient. For $J \gg \Delta B_Z$, J drives rotations around the z-axis leading to oscillations with large visibility, but as J becomes comparable to $\Delta B_Z/2\pi$, ∼30 MHz in this work, the axis of rotation tilts towards the x-axis and the visibility of exchange oscillations becomes small (Bloch sphere in Fig. S1**a**). In order to measure the value of J when it is small, we use a modified pulse sequence where we load the qubit in $|S\rangle$, perform a $\pi/2-$pulse around the x-axis to prepare a state on the y-axis, then turn on J for a time t, and finally perform a $\pi/2-$pulse to project onto $|S\rangle$ (Fig. S1**b**). We use $\pi/2-$pulses around the x-axis because it guarantees good contrast by preparing the qubit in a state that is perpendicular to the axis of rotation for all values of J. We note that this sequence requires a stabilized hyperfine gradient. The observed oscillation is driven by a combination of J and ΔB_Z In order to extract only the component of the splitting due to the exchange interaction, we measure the magnetic field gradient ΔB_Z with each measurement of the splitting and calculate $J(\epsilon) = \sqrt{J_{tot}^2 - (\Delta B_Z)^2}$ where J_{tot} is the observed total frequency.

With an AWG clock frequency of 12 GHz, we can directly measure J_{tot} up to a few GHz. To measure faster oscillations we change the clock rate of the waveform generator, which stretches the pulse, changing the evolution time in small increments. We use adiabatic preparation and readout instead of $\pi/2-$pulses around the x-axis because they do not change when the pulse is stretched by changing the waveform generator clock and do not require a stabilized nuclear gradient (Fig. S1**c**). Using this method, we are able to resolve exchange oscillations exceeding 30GHz. The axis error (see below) associated with using an adiabatic preparation is negligible when measuring such large values of exchange since the angle between the z-axis and axis of revolution $\theta \sim .01 - .001$ radians. We note that for these measurements we use Minicircuits SBLP-467+ low pass filters on the fast detuning gates to prevent Zener tunneling when crossing the $(0,2)$-$(1,1)$ charge transition.

For an exchange echo experiment, there are two ways in which axis errors lead to a reduction in visibility. As in FID, if an adiabatic preparation is used, the axis of rotation is not perpendicular to the prepared state, and we avoid this problem by using $\pi/2$-pulses around the x-axis to prepare and read out the qubit. The second axis error arises from the fact that the axis around which we apply the π-pulse for decoupling is not perpendicular to the axis of rotation. It is possible to mitigate this adverse effect by using a π rotation around the y-axis, although for simplicity in this work we do not. The expected visibility as a function of θ for different sequences is summarized in Table S1.

Rotation Sequence	Ideal Visibility
FID, adiabatic prep	$\cos^2(\theta)$
FID, x-$\pi/2$-prep	1
Echo, adiabatic prep, x-π	$\cos^4(\theta)$
Echo, adiabatic prep, y-π	$\cos^2(\theta)$
Echo, x-$\pi/2$ prep, x-π	$\cos^2(\theta)$
Echo, x-$\pi/2$ prep, y-π	1

TABLE I. The visibility loss associated with the different preparations and π-pulses.

Pulse risetimes in the experimental setup cause the frequency of exchange oscillations to slowly chirp up to a steady value over several nanoseconds. This chirp causes us to underestimate $J(\epsilon)$ in the region where T_2^* is comparable to the time required for J to saturate. Consequently, we are unable to assign unbiased values for $J(\epsilon)$ or T_2^* in the regions of the largest $\frac{dJ}{d\epsilon}$, in this work roughly $-1\text{mV} < \epsilon < 0mV$. Unlike some previous works, ϵ=0 is the detuning at which we measure the state of the qubit and not the degeneracy point between $(0,2)$ and $(1,1)$.

SATURATION OF T_2^*

When $J(\epsilon)$ is small compared to ΔB_Z, T_2^* no longer scales with $dJ/d\epsilon$, but rather saturates at $T^*_{2,nuclear}$ which is limited by the quality of the nuclear feedback. Geometric considerations give

$$(T_2^*)^{-2} = \left(\frac{J}{J_{tot}}\right)^2 \left(T^*_{2,voltage}\right)^{-2} + \left(\frac{\Delta B_Z}{J_{tot}}\right)^2 \left(T^*_{2,nuclear}\right)^{-2} \quad (1)$$

where J is the exchange splitting, $J_{tot} = \sqrt{J^2 + \Delta B_Z^2}$ is the observed frequency, and $T^*_{2,voltage}$ and $T^*_{2,nuclear}$ are the independent coherence times for J and ΔB_Z noise, respectively. We use this form to plot the expected T_2^* and note that this fit has no free parameters since we measure J, ΔB_Z, and $T^*_{2,nuclear}$.

T_2^* AND T_{meas}

Nominally, an FID measurement is sensitive to charge noise from DC to J. However, any given experiment only runs over a period of time T_{meas}, and this introduces and additional low frequency cutoff; noise with a frequency below $1/T_{meas}$ will appear as an offset to J and will not contribute to dephasing. This is particularly relevant for $1/f$ noise, which diverges at DC. In general, as the measurement time increases, the low-frequency cutoff decreases and the observed T_2^* becomes smaller (Fig. S2). This makes it essential to normalize for total measurement time in comparing results between different groups and experiments.

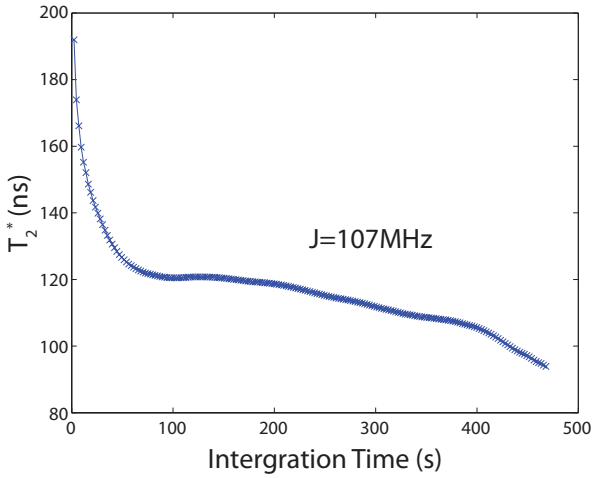

FIG. 2. As we measure exchange oscillations for longer, increasingly low frequency noise contributes to dephasing and T_2^* decreases.

FITTING ECHO DATA

In a typical Hahn echo experiment, we measure the probability of finding a singlet as a function of total evolution time τ and change in length of the second exchange interval δt. In order to self-consistently and reliably fit the data, we simultaneously fit all the echo data for a given value of ϵ. For the power-law noise model, we use the form

$$P_S(\tau,\delta t) = A_0 \cos\left[\omega(\tau)\delta t + \phi(\tau)\right] \times \exp\left[-(\tau/T_2)^{\beta+1} - ((\delta t - t_0(\tau))/T_2^*)^2\right]$$

Allowing ω, ϕ, and the echo center, t_0, to vary with τ allows us to fit in the presence of finite pulse rise times which gives small phase and frequency shifts as a function of τ. Fitting the overall envelope globally through A_0, β, T_2, and T_2^* across many values of τ greatly reduces the probability of encountering local minima during fitting.

In some instances if the $\pi/2$ and π pulses are not tuned perfectly, there may be some "un-echoed" signal at short total evolution times such that $T_2^* \gtrsim \tau$. In this case, we add an additional term to $P_S(\tau,t)$

$$P'_S(\tau,\delta t) = P_S(\tau,\delta t) + A_1 \exp\left[-(\tau/T_2^*)^2\right] \cos\left[\omega(\tau)\delta t + \theta(\tau)\right] \quad (2)$$

Here, the new τ-dependent fit paraemter $\theta(\tau)$ accounts for the phase shift of the unechoed signal due to pulse rise times[25], while A_1 accounts for the magnitude of the un-echoed signal.

DEPHASING FROM OTHER FLUCTUATING PARAMETERS

There is no reason, a priori, to assume that the dephasing present in FID oscillations is due only to fluctuations in ϵ. For example, in a simple avoided crossing model we expect J to depend on the tunnel coupling, T_C, between the QDs. However, the observed linear dependence of T_2^* on $(dJ/d\epsilon)^{-1}$ strongly suggests that fluctuations in ϵ are responsible for the observed dephasing. For T_C to dominate dephasing, we would need $dJ/dT_C \propto dJ/d\epsilon$ for all ϵ, a condition which is not true for the simple avoided crossing model and would generally seem unlikely. The same argument can be repeated for any other parameter that couples to J.

EXTRACTING NOISE POWER

As per Cywinski *et al.*[31], we calculate the amplitude of qubit oscillations by integrating the noise spectrum multiplied by an experiment-specific filter function over all frequencies. For example, for a Hahn echo experiment in the presence of power-law noise $S_\phi(\omega) = \frac{S}{\omega^\beta}$ we find

$$\left(T_2^{echo}\right)^{1+\beta} = \frac{\pi}{2^{-\beta}(-2+2^\beta)S\Gamma(-1-\beta)\sin(\pi\beta/2)} \quad (3)$$

We note that $S_\phi = \frac{1}{2}S_\epsilon(\frac{dJ}{d\epsilon})^2$, where S_ϵ is the ϵ noise spectrum for positive frequencies only. From this we find that $(T_2^{echo})^{-(\beta+1)/2} \propto \frac{dJ}{d\epsilon}$.

For FID experiments, which are dephased by low frequency noise, we assume the noise is quasistatic (much slower than $1/T_2^*$) and normally distributed with variance σ^2. For a given experiment we find the probability of measuring a singlet $P(S) = \int_{-\infty}^{\infty} d\omega e^{-(\omega-\omega_0)^2/2\sigma^2} e^{i\omega t}$, which can be integrated to obtain $P(S) = e^{i\omega_0 t} e^{-t^2\sigma^2/2}$. From here we find $T_2^{*2} = \frac{2}{\sigma^2} = \frac{2}{\epsilon_{RMS}^2(2\pi dJ/d\epsilon)^2}$ where J is in Hertz.

Alternatively, we can consider dephasing from $1/f$ noise during FID experiments, which leads to nearly Gaussian decay. More precisely, for noise described by a noise power $S_\epsilon(\omega) = S_1/\omega$, the decay envelope of FID oscillations is given by $\exp[-\frac{S_1}{4\pi}\left(\frac{dJ}{d\epsilon}\right)^2 t^2 ln\frac{T_{meas}}{2\pi t}]$ where the total measurement time $T_{meas} \approx 5$ minutes provides a low frequeny cutoff to the noise sensitivity[26] (see above). For these measurements, relevant values of t for decay are of order 100 nanoseconds, so we neglect the weak t dependence of the logarithmic term and approximate it by 20. We fit the decay envelope to the form $\exp\left[-(t/T_2^*)^2\right]$, where $T_2^{*2} = \frac{4\pi}{S_1(dJ/d\epsilon)^2 ln\frac{T_{meas}}{2\pi t}}$ and extract $\sqrt{S_\epsilon} = 2\mu\mathrm{V}/\sqrt{f(\mathrm{Hz})}$. We note, however, that the observed dependence of T_2^* on T_{meas} (Fig. S2) is not consistent with simple $1/f$ noise.

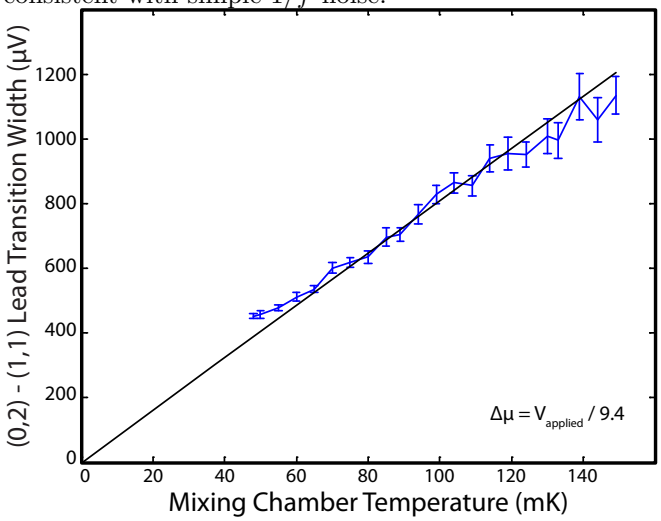

FIG. 3. The $(0,1)$-$(0,2)$ charge transition is thermally broadened, allowing us to determine the electron temperature. The width is calibrated using the mixing chamber temperature at high temperatures. The black line is a best fit, forced through zero width at zero temperature. The "lever-arm" for the fast-RF gates is seen to be 9.4, allowing conversion from gate voltage noise to effective noise at the qubit if desired.

TEMPERATURE DEPENDENCE

All experiments presented are performed in a dilution refrigerator with a base temperature of approximately 50mK. All temperature dependence data are taken by setting the mixing chamber temperature of the dilution refrigerator and waiting sufficient time (30 min) for the system to equilbrate. We monitor the electron temperature as the mixing chamber temperature is changed by measuring the width of a charge transition of the double QD and assuming that the electronic temperature and mixing chamber temperatures are the same at high temperatures (Fig. S3). We find the electronic temperature and lattice temperature (assumed to be the same as that of the mixture) are similar over the range studied and we are therefor unable to differentiate dephasing due to phonons and voltage noise.

MEASURING T_1 AT FINITE ϵ

We measure T_1 as a function of ϵ in two steps. First we prepare a $|S\rangle$, adiabatically ramp to ϵ and wait for a time t, then measure the probability of the resulting state being a singlet, $P_{S|S}$. We then prepare a $|T_0\rangle$ and repeat the process to measure $P_{S|T_0}$. We finally fit $P_{S|S} - P_{S|T_0}$ to an exponential function of t to extract T_1. As seen in Fig. S4, T_1 is much longer than T_2. The nuclear gradient ΔB_Z is stabilized to 30 MHz for this measurement.

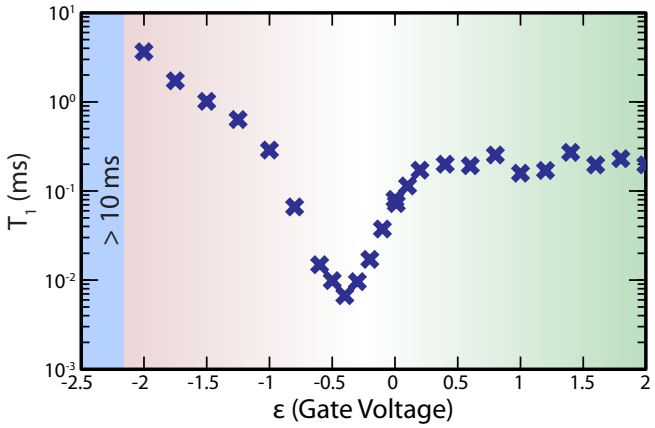

FIG. 4. Although T_1 is a complex function of ϵ, it is much longer than T_2^* and T_2 everywhere.